Ab Initio Mechanism and Multichannel RRKM−TST Rate Constant for the Reaction of $Cl(^2P)$ with CH_2CO (Ketene)

Hua Hou, Baoshan Wang,* and Yueshu Gu

School of Chemistry, Shandong University, Jinan, Shandong 250100, People's Republic of China

Received: August 11, 1999; In Final Form: November 1, 1999

The potential energy surface for the most important pathways of the reaction between $Cl(^2P)$ and ketene has been studied using the ab initio G2(MP2) method. A variety of possible complexes and saddle points along the minimum energy reaction paths have been characterized at the UMP2(full)/6-31G(d,p) level. The calculations reveal that the addition−elimination mechanism dominates the Cl + CH_2CO reaction and the direct hydrogen abstraction pathway is negligible. It is interesting to note that the addition reaction starts by the formation of a p−π complex (PπC), and subsequently the chlorinated acetyl radical $CH_2ClCO(^2A')$ and the chloroformyl methyl radical $CH_2CClO(^2A'')$ are formed through the isomerization of PπC. The C−C bond scission of $CH_2ClCO(^2A')$ leads to the products CO and CH_2Cl. The three-center HCl elimination from PπC, occurring via a high energy barrier (TS3) and a weakly bound hydrogen bonding (HBC1), was proposed to account for the minor yield of the HCl + HCCO observed experimentally. Multichannel RRKM−TST calculation has been carried out for the total and individual rate constants for various channels using the ab initio data. The "loose transition state" in the barrierless reaction entrance was determined by fitting the known experimental rate constant at 295 K. The kinetic calculations in this work can explain reasonably all the previous experimental results. In the temperature range 300−1500 K and the atmospheric pressure of N_2, the total rate constants exhibit negative temperature dependence and can be fitted to the expression $k(T) = (1.0 \pm 0.2) \times 10^{-15} T^{-1.58\pm0.02} \exp(-565 \pm 2/T)$ cm^3 molecule^{-1} s^{-1}. Meanwhile, the rate constants show the typical fall-off behavior in the pressure range 10^3−10^8 Torr. At lower pressures ($P < 10^3$ Torr), the rate constants are pressure independent and the major products are CO and CH_2Cl over the whole temperature range of interest. At the high-pressure limit ($P > 10^8$ Torr), the stabilization of PπC dominates the reaction. It is found that two radical products, namely $CH_2ClCO(^2A')$ and $CH_2CClO(^2A'')$, might be detectable in the fall-off region.

I. Introduction

The elementary reactions of the ketene molecule (CH_2CO) with reactive atoms and radicals in the gas phase are of considerable importance in combustion of hydrocarbons. The kinetics and products of the reactions of CH_2CO with H, $O(^3P)$, F, Cl, OH, CN, and NCO have been more or less investigated experimentally.[1−14] The Cl + CH_2CO reaction is of special interest because of its distinctive reaction mechanism. A few product channels are possible in the Cl + CH_2CO reaction, namely

$$\mathrm{Cl} + \mathrm{CH_2CO} \rightarrow \mathrm{CO} + \mathrm{CH_2Cl}\ \Delta H^\circ_0 = -16.7\ \text{kcal/mol} \quad \text{(I)}$$

$$\rightarrow \mathrm{HCl} + \mathrm{HCCO}\ \Delta H^\circ_0 = 2.8\ \text{kcal/mol} \quad \text{(II)}$$

$$\rightarrow \mathrm{H} + \mathrm{CHClCO}\ \Delta H^\circ_0 = 24.4\ \text{kcal/mol} \quad \text{(III)}$$

$$\rightarrow \mathrm{OH} + \mathrm{ClCCH}\ \Delta H^\circ_0 = 44.1\ \text{kcal/mol} \quad \text{(IV)}$$

$$\rightarrow \mathrm{CHCl} + \mathrm{HCO}\ \Delta H^\circ_0 = 70.7\ \text{kcal/mol} \quad \text{(V)}$$

$$\rightarrow \mathrm{CH_2} + \mathrm{ClCO}\ \Delta H^\circ_0 = 72.4\ \text{kcal/mol} \quad \text{(VI)}$$

where the values of ΔH°_0 were calculated using the enthalpies of formation in the literature.[15,16] It is evident that channels IV, V, and VI are highly endothermic and can be ruled out. Therefore, in this paper we have focused on the study of channels I, II, and III and several isomerization channels of various intermediates involved in the Cl + CH_2CO reaction.

Experimentally, the available kinetic information about the Cl + CH_2CO reaction is only the rate constant at room temperature. An earlier direct measurement by Ebrecht et al. in an isothermal flow reactor with a mass spectrometric detection device yielded a rate constant of 6.8×10^{-11} cm^3 molecule^{-1} s^{-1} at 294 K in 0.75 Torr of helium.[9] Recently, Wallington et al. studied the Cl + CH_2CO reaction using a FTIR spectrometer/smog chamber apparatus and the relative rate technique.[10] The rate constant was determined to be $(2.7 \pm 0.5) \times 10^{-10}$ cm^3 molecule^{-1} s^{-1} at 295 K, which is 4 times larger than that reported by Ebrecht et al.[9] Moreover, the rate constant was found to be independent of total pressure over the range 1−700 Torr of air diluent. The latest real-time kinetic measurement by Maricq et al.[11] using laser-flash photolysis/diode laser spectroscopy supported the rate determination by Wallington et al.[10] In the total pressure of 10−200 Torr of N_2, the rate constant was measured to range from 2×10^{-10} to 3×10^{-10} cm^3 molecule^{-1} s^{-1} at 295 K. Moreover, at the temperatures of 235 and 353 K, the rate constants almost remain unchanged from those at 295 K.

In 1994, Grussdorf et al. measured the absolute yields of the primary products of the Cl + CH_2CO reaction in about 1 Torr of helium at room temperature using a discharge flow/far

* Corresponding author. E-mail: guojz@icm.sdu.edu.cn.

10.1021/jp992829+ CCC: $19.00
Published on Web 12/22/1999

infrared laser magnetic resonance spectrometer.[12] They found that only channel I is observable. The production of CO and CH_2Cl has a branching ratio of 0.97 ± 0.07. The other minor products were assumed to be HCl and HCCO with a branching ratio of less than 0.01. Therefore, they concluded that the addition−elimination mechanism dominates the reaction and the hydrogen abstraction mechanism is negligible.

There is no quantitative dynamic measurement for the Cl + CH_2CO reaction. The only dynamic information is that the CO molecule was mentioned to be born in its vibrational ground state.[11] However, whether the CH_2Cl fragment is vibrationally excited is still unknown.

Unambiguously, the previous experimental information about the Cl + CH_2CO reaction is far from satisfactory. Therefore, a theoretical study of this important reaction is apposite. It is well-known that ab initio molecular orbital (MO) theory plays an important role not only in understanding overall reaction mechanisms but also in interpreting and predicting experimental results. There is no theoretical study of the Cl + CH_2CO reaction to date except a rough calculation for $\Delta H°_{298}$ of the CH_2ClCO radical at the MP2/6-31G(d,p) level.[10]

In this paper we present an extensive theoretical study of the Cl + CH_2CO reaction. The detailed reaction mechanism is revealed for the first time. The calculations show that the reaction mechanism is much more sophisticated than that expected previously. We used multichannel RRKM and transition state theory (TST) with the ab initio potential surface data to deduce the rate constants of the title reaction over wide temperature and pressure ranges. The results shed new light on future experiments or dynamical studies.

II. Computations

Ab initio calculations were performed using the Gaussian 94 program.[17] The geometries of reactants, transition states, intermediates, and products were optimized at the UMP2(full) level[18] with the 6-31G(d,p) basis set. It has been shown that this level of theory can give a proper reproduction of the experimental data for the molecular structure and vibrational IR spectrum of ketene.[19] A further discussion about the basis sets applied in the optimizations will be given below. The vibrational frequencies employed to characterize stationary points, zero-point energies (ZPE), and rate constant calculations have also been calculated at this level of theory and scaled by a factor of 0.95 to partly eliminate known systematic errors.[20] The number of imaginary frequencies (0 or 1) indicates whether a minimum or a transition state has been located. The transition states were subjected to intrinsic reaction coordinate (IRC)[21,22] calculations (using the default step size) to facilitate connection with minima along the reaction paths. Each IRC terminated upon reaching a minimum using the default criterion.

The major problem in the application of unrestricted single determinant reference wave function is that of contamination with higher spin states. The severe spin contamination could lead to a deteriorated estimation of the barrier height.[23,24] We have examined the spin contamination before and after annihilation for the radical species and transition states involved in the Cl + CH_2CO reaction. The expectation values of $\langle S^2 \rangle$ range from 0.90 to 0.75 before annihilation, and after annihilation $\langle S^2 \rangle$ is 0.75 (the exact value for a pure doublet). This suggests that the wave function is not severely contaminated by states of higher multiplicity.[25,26]

To obtain more reliable energies of various stationary points on the potential energy surface (PES), we used the popular and inexpensive G2(MP2)[27] method for the present four heavy atom system. As indicated by the good agreement of the calculated heats of reaction with the experimental values, the G2(MP2) energetics are expected to be reliable with a likely error of ±2 kcal/mol.

The rate constants were evaluated by the multichannel Rice−Ramsperger−Kassel−Marcus (RRKM) and transition state theory (TST).[28,29] The calculations are fully detailed in section III.4.

III. Results and Discussion

Two kinds of mechanisms for the Cl + CH_2CO reaction were examined in this study. One is the addition−elimination mechanism, and the other is the direct hydrogen abstraction mechanism. The optimized geometries of various key species involved in these two mechanisms are shown in Figure 1. The corresponding vibrational frequencies and energies are listed in Tables 1 and 2, respectively. The profile of the potential energy surface at the UMP2(full)/6-31G(d,p) level (without ZPE correction) is shown in Figure 2. For clarity, these two mechanisms will be discussed separately in the following sections. The energies used in the discussion have included the ZPE corrections at the UMP2(full)/6-31G(d,p) level unless otherwise stated.

1. Addition−Elimination Mechanism. The highly electrophilic character of Cl(^{2}P) atom and the molecular orbital configuration of ketene should govern the site of initial attack. The highest filled π orbital of ketene, which is perpendicular to the molecular plane, shows a node on the central atom (the carbonyl carbon) of the π system. The majority of the electron density is located on the methylene carbon.[30] Therefore, the chlorine addition to ketene would prefer to occur at the methylene carbon of the π system.

A. Formation of the p−π Complex (PπC). Previous experimental studies suggested that the addition reaction of Cl with CH_2CO starts by the direct formation of the chloroacetyl radical (CH_2ClCO).[9−12] However, we found that this argument is untenable. At the UMP2(full)/6-31G(d,p) level, the potential energy surface for the attack of Cl(^{2}P) upon the methylene carbon of CH_2CO within ^{2}A′ state of C_s symmetry has been scanned using the restricted optimization method. The forming CCl bond was fixed at the values from 5.3 to 2.3 Å with the interval of 0.1 Å, and the other geometrical parameters were optimized for each value of CCl. The potential curve obtained is shown in Figure 3. It is obvious that a minimum exists at the CCl distance of 2.4−2.5 Å. This minimum was further fully optimized and is shown in Figure 1 as PπC(^{2}A′). The frequency analysis indicates that PπC(^{2}A′) is a true local minimum and appears to be a typical $p-\pi$ complex, occurring between the p orbitals of chlorine atom and the symbol π system of the ketene molecule. The CCl bond length is 2.443 Å. Compared with the structure of ketene, the CC bond is stretched by 0.026 Å, and the CO bond is shortened by 0.016 Å. The CCO structure is slightly bent. However, both the CC and CO bonds retain their double bond character because the unpaired electron in the complex is still located mainly on the Cl atom.

PπC(^{2}A′) was also optimized at the higher QCISD/6-31G(d) level to confirm the existence of such a complex. The geometrical parameters obtained are also listed in Figure 1. The vibrational frequencies at the QCISD/6-31G(d) level (see Table 1) once again reveal that PπC(^{2}A′) is a true minimum. The formation of PπC(^{2}A′) from the reactants Cl + CH_2CO is a barrierless process, as indicated by the potential energy curve in Figure 3. The binding energy of PπC(^{2}A′) is calculated to be 10.1 kcal/mol at the G2(MP2) level.

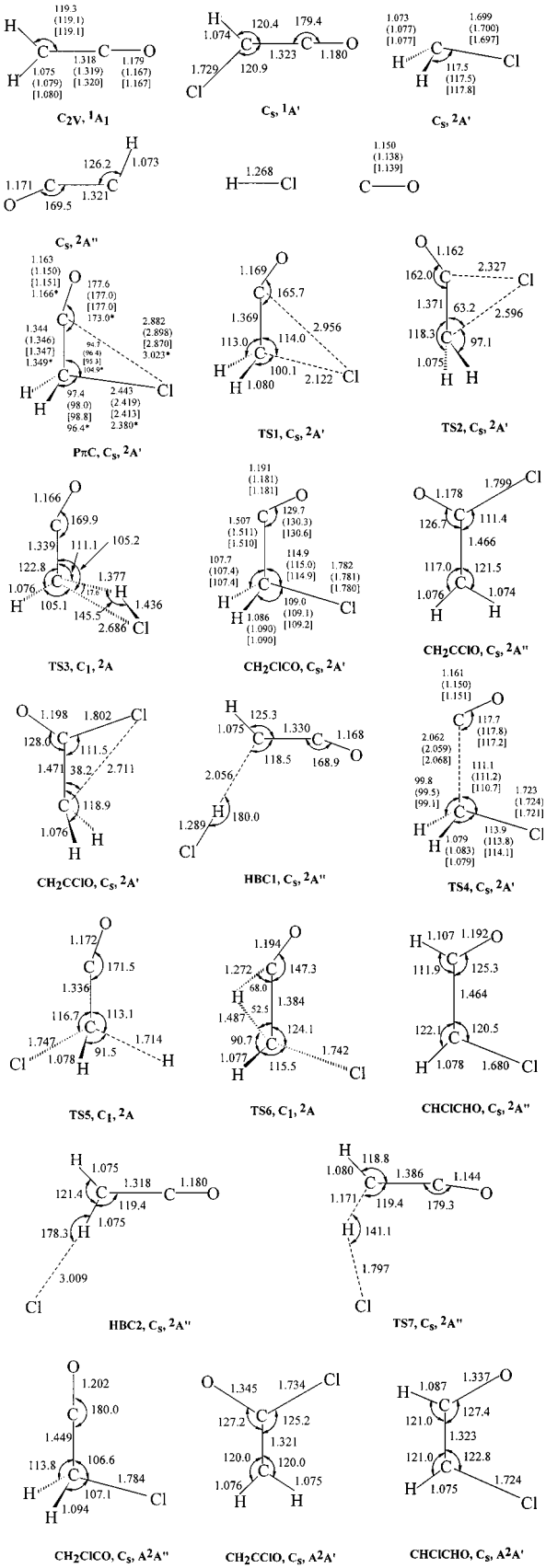

Figure 1. UMP2(full)/6-31G(d,p) optimized geometries of the reactants, products, various intermediates, and transition states (TS) for the Cl + CH_2CO reaction. The values in parentheses correspond to the UMP2(full)/6-311G(d,p) level. The values in square brackets correspond to the UMP2(full)/6-311+G(d,p) level. The numbers with asterisks for PπC(^{2}A′) are obtained at the UQCISD/6-31G(d) level. Bond distances are in angstroms and angles are in degrees.

B. Dissociation and Isomerization of PπC(^{2}A′). The optimization and IRC calculation at the UMP2(full)/6-31G(d,p) level reveal three kinds of reaction pathways of PπC(^{2}A′), leading to chloroacetyl CH_2ClCO(^{2}A′), chloroformylmethyl CH_2CClO-(^{2}A″), and HCl + HCCO, respectively.

TS1 is the transition state for the isomerization from PπC-(^{2}A′) to CH_2ClCO(^{2}A′). In TS1, the CCl bond is shortened to 2.122 Å. The CC bond is stretched to 1.369 Å and the CCO structure is more bent. TS1 is a rather early barrier because the rather short CC bond suggests its double bond character. However, spin density analysis shows that the unpaired electron in TS1 begins to be delocalized from chlorine to carbonyl carbon. In the product CH_2ClCO(^{2}A′), the CC bond becomes a single bond as indicated by its long distance (1.507 Å), and the radical center is moved to the π orbital of the carbonyl carbon. Both TS1 and CH_2ClCO have C_s symmetry and ^{2}A′ states. At the UMP2(full)/6-31G(d,p) level, the energy of TS1 is calculated to be 2.1 kcal/mol higher than that of PπC. However, at the G2(MP2) level, the energy of TS1 becomes about 1.1 kcal/mol lower than that of PπC. This may be caused by the fact that the energy calculated at the G2(MP2) level for a MP2-optimized geometry does not correspond exactly to the top of the saddle point. As will be shown below, at the UMP2(full) level with a more flexible basis set such as 6-311+G(d,p), this transition state disappears effectively. The energy of CH_2ClCO is about 12.0 kcal/mol lower than that of PπC at the G2(MP2) level. Therefore, the radical complex PπC should be unstable with respect to CH_2ClCO both thermodynamically and kinetically.

PπC can rearrange to CH_2CClO via transition state TS2. In TS2, the breaking CCl bond is elongated by 0.153 Å and the CCCl angle decreases to 63.2°. Simultaneously, the Cl atom and the carbonyl carbon atom tend to form a bond as indicated by the shortened CCl distance (2.327 Å). The IRC calculation confirms that TS2 does connect PπC(^{2}A′) with CH_2CClO(^{2}A″). However, in the product side, the IRC job will terminate upon reaching a structure CH_2CClO(^{2}A′) if the C_s symmetry is always retained in the calculation. When the imposed C_s symmetry constraint is released in the IRC calculation, CH_2CClO(^{2}A″) is arrived at directly. This implies that the exit of TS2 prefers to be of C_1 symmetry. CH_2CClO(^{2}A′) corresponds to the saddle point of internal rotation around the CC axis, as indicated by an imaginary frequency of 251 cm^{-1} in Table 1. CH_2CClO-(^{2}A″) can be considered as chloroformylmethyl radical. It has a long CC single bond. The unpaired electron is localized on the methylene carbon. The transition state TS2 has a rather early character, in accordance with the exothermicity of this rearrangement channel. At the UMP2(full)/6-31G(d,p) level, the barrier height is 4.7 kcal/mol. However, this value is reduced to as little as 0.9 kcal/mol at the G2(MP2) level.

It is worth noting that CH_2CClO(^{2}A″) cannot correlate adiabatically with the reactants Cl + CH_2CO on the ^{2}A″ ground PES. The potential energy curve describing the CCl bond scission of CH_2CClO(^{2}A″) shows that the energy of system exceeds that of the reactants significantly while the CCl bond breaks (see Supporting Information). CH_2CClO(^{2}A″) might correlate with an excited potential surface in the reactant region.

PπC can decompose to HCl + HCCO via three-center transition state TS3 and a hydrogen-bonded complex (HBC1). At first sight this intramolecular HCl elimination is symmetry-forbidden because PπC has ^{2}A′ electronic state but the overall electronic states of both HBC1 and HCl($^1\Sigma^+$) + HCCO (^{2}A″) are ^{2}A″. However, this constraint does not exist because the symmetry breaks along the reaction path and the transition state TS3 indeed has no symmetry. IRC calculation confirmed the

TABLE 1: Harmonic Vibrational Frequencies (in cm^{-1}) for Various Species Involved in the Reaction of Cl(^{2}P) with CH_2CO

species	vibrational frequencies[a]
CH_2CO	439, 518, 584, 1014, 1173, 1459, 2245, 3299, 3413
$[CH_2CO]$[b]	443, 503, 589, 992, 1159, 1415, 2240, 3239, 3351
(CH_2CO)[c]	441, 475, 578, 988, 1156, 1412, 2225, 3237, 3349
CHClCO	187, 493, 507, 593, 851, 1167, 1362, 2240, 3354
CH_2Cl	336, 886, 1057, 1506, 3293, 3447
$[CH_2Cl]$[b]	244, 880, 1047, 1473, 3243, 3398
(CH_2Cl)[c]	159, 884, 1047, 1474, 3242, 3397
HCCO	537, 616, 694, 1299, 2463, 3399
CO	2125
[CO][b]	2139
(CO)[c]	2127
HCl	3127
PπC	93, 271, 423, 437, 532, 724, 1032, 1153, 1448, 2249, 3287, 3406
[PπC][b]	93, 286, 426, 480, 560, 755, 1012, 1132, 1399, 2265, 3227, 3346
PπC[d]	*94, 147, 421, 446, 512, 823, 1055, 1121, 1448, 2197, 3224, 3325*
$CH_2ClCO(^2A')$	177, 201, 612, 773, 836, 883, 1234, 1336, 1484, 1989, 3186, 3256
$[CH_2ClCO(^2A')]$[b]	182, 199, 612, 771, 819, 868, 1224, 1319, 1441, 1965, 3143, 3207
$CH_2CClO(^2A'')$	198, 374, 457, 572, 626, 712, 1033, 1164, 1505, 2309, 3287, 3432
$CH_2CClO(^2A')$	251i,[e] 287, 451, 473, 512, 666, 1041, 1080, 1484, 2001, 3284, 3414
HBC1	45, 140, 229, 484, 508, 582, 599, 792, 1217, 2420, 2820, 3376
$CHClCHO(^2A'')$	221, 280, 507, 713, 836, 1080, 1095, 1392, 1469, 2065, 2999, 3323
HBC2	17, 54, 66, 442, 520, 586, 1016, 1174, 1461, 2244, 3298, 3413
TS1	503i, 149, 400, 478, 697, 1026, 1069, 1116, 1453, 2185, 3247, 3348
TS2	513i, 189, 314, 363, 470, 616, 1041, 1067, 1452, 2204, 3298, 3429
TS3	1480i, 88, 421, 482, 561, 596, 865, 1064, 1154, 1243, 2388, 3362
TS4	550i, 71,[f] 132, 378, 605, 815, 1027, 1109, 1496, 2026, 3240, 3368
[TS4][b]	542i, 71, 133, 382, 586, 808, 1001, 1101, 1466, 2036, 3190, 3314
TS5	1498i, 182, 367, 554, 608, 651, 837, 918, 1159, 1350, 2224, 3312
TS6	1452i, 182, 562, 656, 667, 766, 1180, 1222, 1375, 2054, 2360, 3342
TS7	666i, 559i, 173, 356, 494, 816, 890, 1072, 1101, 2046, 2494, 3321
$CH_2ClCO(A^{2''})$	947i, 181, 539, 796, 933, 979, 1355, 1397, 1575, 2262, 3065, 3100
$CH_2CClO(A^{2'})$	4944i, 349, 395, 569, 696, 830, 982, 1223, 1476, 2466, 3311, 3404
$CHClCHO(A^{2'})$	2172i, 190, 494, 645, 832, 928, 1104, 1240, 1399, 2406, 3248, 3369

[a] The UMP2(full)/6-31G(d,p) values unless otherwise stated. [b] The frequencies are calculated at the UMP2(full)/6-311G(d,p) level. [c] The frequencies are calculated at the UMP2(full)/6-311+G(d,p) level. [d] The numerical frequencies at the QCISD/6-31G(d) level. [e] *i* represents imaginary frequency. [f] This value has been substituted by a free rotation around the C−C axis in the RRKM calculation. The reduced moment of inertia for the free rotation was computed to be 5.7 amu.

TABLE 2: Relative Energies and ZPE Corrections (in kcal/mol) for Various Species through the Cl + CH_2CO Reaction

species	$\langle S^2\rangle$[a]	ZPE	MP2(full)[b]	G2(MP2)[c]	exptl[d]
Cl(^{2}P) + $CH_2CO(^1A_1)$	0.75, 0.0	19.2	0.0	0.0	
CO ($^1\Sigma^+$) + CH_2Cl ($^2A'$)	0.0, 0.76	17.2	−13.6	−18.3	−16.7 ± 2.0
HCl($^1\Sigma^+$) + HCCO ($^2A''$)	0.0, 0.81	16.5	11.8	2.8	2.8 ± 2.0
H(^{2}S) + CHClCO ($^1A'$)	0.75, 0.0	14.6	25.4	25.3	24.4 ± 2.0
PπC, C_s, $^2A'$	0.77	20.4	−7.3	−10.1	
CH_2ClCO, C_s, $^2A'$	0.77	21.7	−18.3	−22.0	
CH_2CClO, C_s, $^2A''$	0.83	21.3	−19.7	−27.9	
CH_2CClO, C_s, $^2A'$	0.76	20.0	−17.7	−21.5	
HBC1, C_s, $^2A''$	0.80	17.9	7.2	0.2	
CHClCHO, C_s, $^2A''$	0.87	21.7	−8.9	−20.5	
HBC2, C_s, $^2A''$	0.76	19.4	−0.4	−0.7	
TS1, C_s, $^2A'$	0.83	20.6	−5.2	−11.2	
TS2, C_s, $^2A'$	0.83	19.6	−2.6	−9.2	
TS3, C_1, ^2A	0.79	16.6	13.7	5.9	
TS4, C_s, $^2A'$	0.81	19.4	−2.7	−9.4	
TS5, C_1, ^2A	0.90	16.5	39.9	31.0	
TS6, C_1, ^2A	0.82	19.5	30.9	20.4	
TS7, C_s, $^2A''$	0.79	17.3	26.0	16.8	

[a] The expectation value of $\langle S^2\rangle$ before projection. Values after projection are 0.75 for all doublets. [b] The relative energies calculated at the UMP2(full)/6-31G(d,p) level with ZPE corrections. The total energy (E_0, in hartrees) of Cl + CH_2CO is −611.707 73. [c] The relative energies calculated at the G2(MP2) level. The total energy (E_0, in hartrees) of Cl + CH_2CO is −612.032 17. [d] The experimental data from refs 15 and 16.

connection of PπC(^{2}A′) with HBC1(^{2}A″) via unsymmetric TS3. This decomposition channel involves a high energy barrier, 16.0 kcal/mol at the G2(MP2) level, which is even 5.9 kcal/mol higher than the total energy of the reactants Cl + CH_2CO, so the HCl elimination from PπC is energetically less feasible than its two rearrangement channels. HBC1 is a weakly hydrogen bonded complex between the HCl molecule and the HCCO radical. The hydrogen bonding occurs between the hydrogen atom of HCl and the methylidyne carbon of HCCO. The ClHC structure is found to be linear and the H···C distance is 2.056 Å. The binding energy (D_0) of HBC1 is 2.6 kcal/mol at the G2(MP2) level.

C. Dissociation and Isomerization of $CH_2ClCO(^2A')$. The significant internal energy of CH_2ClCO drives it to dissociate into various products. The energetically most favorable decomposition pathway of CH_2ClCO occurs through CC bond cleav-

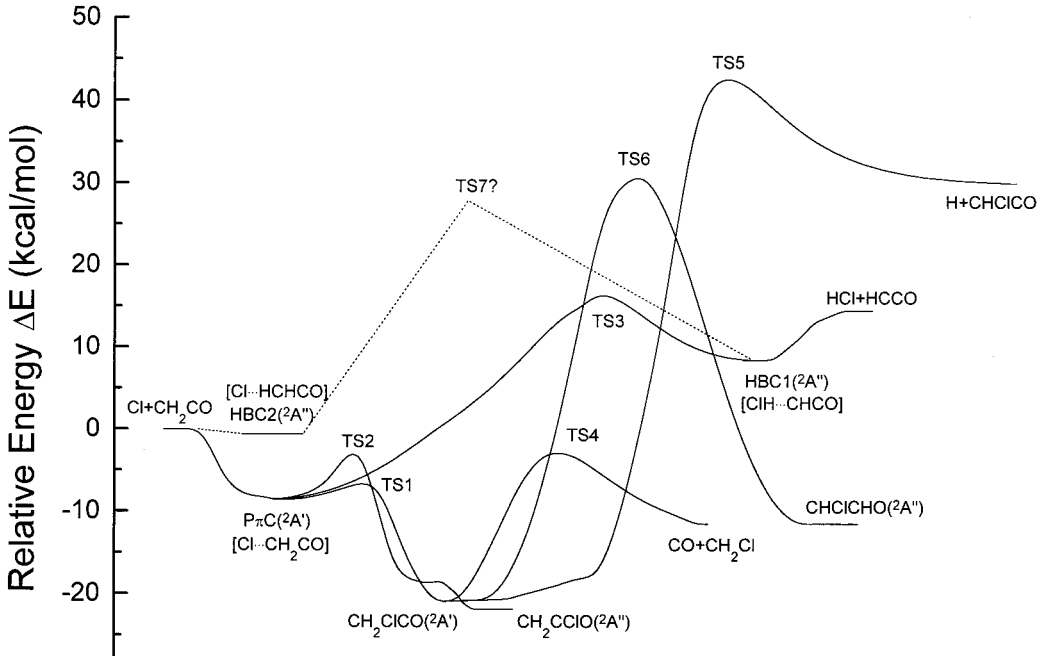

Figure 2. Profile of the potential energy surface at the UMP2(full)/6-31G(d,p) level of theory (without ZPE correction) for the most important mechanism of the Cl + CH_2CO reaction. Note that TS7 is only a second-order saddle point.

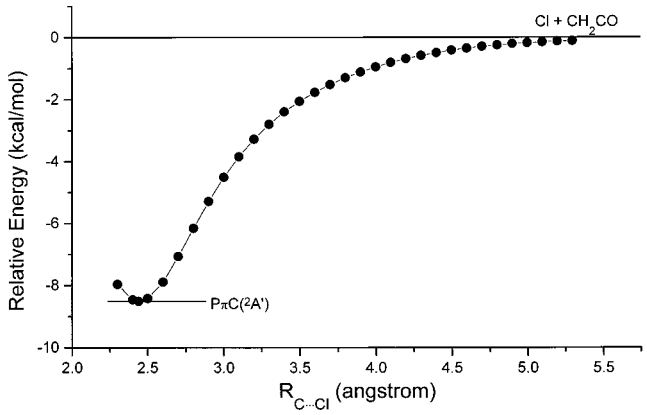

Figure 3. Potential energy curve for the formation of p−π complex from Cl + CH_2CO on the $^2A'$ potential surface. The energies were calculated at the UMP2(full)/6-31G(d,p) level. The forming CCl bond was fixed at the values from 5.3 to 2.3 Å with the interval of 0.1 Å, and other geometrical parameters were optimized for each value of CCl.

age, forming $CO(^1\Sigma^+)$ and $CH_2Cl(^2A')$ via transition state TS4($^2A'$). The barrier height is 12.6 kcal/mol at the G2(MP2) level. The energy of TS4 is 9.4 kcal/mol lower than that of the reactants Cl + CH_2CO. The overall reaction is exothermic by 18.3 kcal/mol. However, the $CH_2ClCO \rightarrow CO + CH_2Cl$ channel is endothermic, and thus the transition state TS4 has a rather late character. The breaking CC bond is elongated by 0.555 Å. The length of CO bond is nearly equal to that of the free CO molecule. Consequently, the vibrationally cold CO molecule may be born, as observed in the experiment. The excess energy of the system may be released either into the CH_2Cl fragment or as relative translational energy or both.

The other symmetry-allowed decomposition channel of CH_2ClCO produces H atom and chlorinated ketene (CHClCO) via transition state TS5. This reaction path is highly endothermic by 25.3 kcal/mol. Therefore, TS5 is a productlike barrier. The breaking CH bond, for instance, is stretched by 58%. The barrier height is 53.0 kcal/mol at the G2(MP2) level. Evidently, this CH cleavage channel is energetically less favorable.

We have also examined the intramolecular 1,2-H shift pathway of CH_2ClCO via transition state TS6. The final product is found to be formylchloromethyl radical $CHClCHO(^2A'')$. As can be seen from the geometrical parameters of CHClCHO, it has a CC single bond and a CO double bond. The unpaired electron is located at the chloromethylene carbon. CHClCHO has a $^2A''$ electronic state of C_s symmetry, so the transition state TS6 involved has to be unsymmetrical to connect $CH_2ClCO(^2A')$ with $CHClCHO(^2A'')$. The IRC calculation confirmed this type of connection. The energy of CHClCHO is slightly higher than that of CH_2ClCO, and the $CH_2ClCO \rightarrow$ CHClCHO isomerization is nearly thermoneutral. However, the energy barrier of 42.4 kcal/mol for this H-migration path is rather high. The energy of TS6 is 20.4 kcal/mol higher than that of the reactants Cl + CH_2CO at the G2(MP2) level, so this hydrogen migration channel of CH_2ClCO is not feasible kinetically.

Although the intermediate CH_2CClO also has a large amount of excess internal energy, neither decomposition nor isomerization can occur readily because there is no energetically accessible product channel. Therefore, $CH_2CClO(^2A'')$ prefers to be deactivated by bath gases or rearrange back to the p−π complex.

We have also examined tentatively several excited electronic states of CH_2ClCO, CH_2CClO, and CHClCHO. The optimized structures are shown in Figure 1 as $CH_2ClCO(^2A'')$, $CH_2CClO(^2A')$, and $CHClCHO(^2A')$, respectively. It is evident that the geometries of these excited states are significantly different from those of the ground states. However, the frequency analysis shows that each excited electronic state has one abnormally large imaginary frequency (Table 1). The imaginary vibrational mode corresponds to the out-of-plane motion. It implies that these structures should not retain C_s symmetry. The energies of these excited electronic states are much higher than those of the ground states and the reactants. Therefore, these excited species might play a minor or negligible role in the Cl + CH_2CO reaction. The conclusive description of these excited species is quite computationally intensive and thus is reserved for future study.

TABLE 3: Dependence of the G2(MP2) Total Energies (in hartrees) and Relative Energies (in Parentheses, in kcal/mol) on the Different Basis Sets Employed in the UMP2(full) Optimizations[a]

species	6-31G(d,p) (74)[b]	6-311G(d,p) (92)[b]	6-311+G(d,p) (108)[b]
$Cl + CH_2CO$	−612.032 17 (0.0)	−612.032 50 (0.0)	−612.032 50 (0.0)
$P\pi C(^2A')$	−612.048 27 (−10.1)	−612.048 68 (−10.2)	−612.048 67 (−10.1)
$CH_2ClCO(^2A')$	−612.067 18 (−22.0)	−612.067 43 (−21.9)	−612.067 43 (−21.9)
$TS4(^2A')$	−612.047 09 (−9.4)	−612.047 39 (−9.3)	−612.047 33 (−9.3)
$CH_2Cl + CO$	−612.061 29 (−18.3)	−612.061 85 (−18.4)	−612.061 86 (−18.4)

[a] The UMP2(full)/6-31G(d,p) ZPEs (scaled by 0.95) are included in all the G2(MP2) total energies since the ZPEs are nearly independent of basis sets. [b] Number of basis functions of the basis set used in the optimization.

2. Direct Abstraction Mechanism. Experimentally, the hydrogen abstraction of CH_2CO by Cl has been proposed to account for the minor yield of HCl.[9−12] Because the products $HCl(^1\Sigma^+)$ + $HCCO(^2A'')$ can correlate adiabatically with the reactants Cl(^{2}P) + $CH_2CO(^1A_1)$ and the reaction is slightly endothermic by 2.8 kcal/mol, the minor yield of HCl molecules suggests that the hydrogen abstraction reaction has to surmount a high barrier.

Along the reaction path, a local minimum, namely HBC2 as shown in Figure 1, was first found. HBC2 has a nearly linear hydrogen bonding between the Cl atom and one of the hydrogen atoms of ketene. This complex is rather weak as indicated by the long Cl···H bond. The binding energy is only 0.7 kcal/mol at the G2(MP2) level. It is worth noting that the primary product in the abstraction reaction should be the hydrogen-bonded complex between HCl and HCCO, i.e., HBC1. The final products HCl and HCCO are born by the decomposition of HBC1.

To search for the saddle point along the reaction path, the potential energy surface corresponding to the Cl···H bond formation and the C···H bond cleavage was scanned at the UMP2(full)/6-31G(d,p) level using the restricted optimization method. In this kind of calculation, the ClHC angle was fixed at 180.0°. The ClH distance was fixed at the values from 1.3 to 2.3 Å with the interval of 0.1 Å, and the HC distance was fixed at the values from 1.1 to 1.6 Å. The other geometrical parameters were optimized. The contour plot of PES is shown in the Supporting Information. It indicates that a saddle point exists at R_{ClH} = 1.8 Å and R_{CH} = 1.2 Å. However, the corresponding transition state cannot be optimized if the ClHC angle is still fixed at 180° because there is no desired negative eigenvalue in the Hessian matrix. When the ClHC angle is also optimized but the supermolecule is still constrained to be planar, a "transition state", namely TS7, can be located at the UMP2-(full)/6-31G(d,p) level. The vibrational frequency analysis, however, shows that TS7 is actually a second-order saddle point with two imaginary frequencies as indicated in Table 1. The larger imaginary frequency, 666 cm^{-1}, results from the motion along the reaction coordinate (the eigenvector $\hat{e} = -0.49R_{ClH} + 0.33R_{CH} - 0.11R_{CC} + 0.65A_{ClHC}$), and the smaller imaginary frequency corresponds to an out-of-plane rotation ($\hat{e} = 0.51D_{ClHCC} + 0.85D_{ClHCH}$). When the C_s symmetry constraint is removed, the optimization always converges to the transition state TS3, even though the geometry of TS7 is far different from that of TS3. Improving the levels of theory employed cannot circumvent this difficulty effectively. The energy of TS7 is much higher than those of the reactants and TS3. At the G2-(MP2) level, the energy difference between TS7 and TS3 is about 11 kcal/mol.

Although only a second-order top is found along the direct hydrogen abstraction path, two qualitative results still can be drawn on the basis of the calculated energetics. One is that the direct hydrogen abstraction path may play a minor or negligible role in the overall reaction of Cl with CH_2CO. The other is that the minor product HCl detected experimentally in the $Cl + CH_2$-CO reaction prefers to result from the three-center HCl elimination of the p−π complex rather than from the direct hydrogen abstraction of CH_2CO by Cl atom.

3. Dependence of the ab Initio Results on the Basis Set. As suggested by one of the referees, it is valuable to explore the influence of different basis sets on the ab initio results since only a quite small basis set [6-31G(d,p)] was used in the optimizations. For the present six-atom system including four heavy atoms, the UMP2(full) calculation with more flexible basis set is computationally more intensive. Therefore, only the most important reaction channel [$Cl + CH_2CO \rightarrow CO + CH_2$-Cl (I)] was examined because of the limitation of our computational resources. As mentioned above, the energy of TS1 is lower than that of the p−π complex at the G2(MP2) level. In fact, this transition state disappears at the UMP2(full)/6-311+G-(d,p) level. Hence, only the species involved in the pathway $Cl + CH_2CO \rightarrow P\pi C \rightarrow CH_2ClCO(^2A') \rightarrow TS3 \rightarrow CO + CH_2Cl$ are necessary to be considered. Besides the 6-31G(d,p) basis set, two larger basis sets were applied in the UMP2(full) optimization. One is the three-split-valence type basis set 6-311G(d,p) and the other is the 6-311+G(d,p) basis set which includes diffuse functions. The geometries and harmonic frequencies of all the stationary points involved in this channel were calculated using the UMP2(full) method with these three types of basis sets. Note that the UMP2(full)/6-311+G(d,p) frequencies cannot be achieved for intermediates and transition states. The geometrical parameters are shown in Figure 1. The vibrational frequencies are summarized in Table 1. The G2-(MP2) energies were also calculated on the basis of the geometries obtained at three levels. The results are listed in Table 3 for the purpose of comparison.

Three conclusions can be drawn straightforwardly from these calculations. First, the basis sets have little effect on the UMP2-optimized geometrical parameters for various species. As shown in Figure 1, from the smaller 6-31G(d,p) to the larger 6-311G-(d,p) and 6-311+G(d,p) basis sets, the change of bond distance is less than 0.03 Å and the change of bond angle does not exceed 2°. Second, the harmonic vibrational frequencies of various species are barely influenced by different basis sets. For each species, the average deviation of each separated normal vibrational frequency is less than 5% except the umbrella vibration mode of CH_2Cl radical, so the ZPEs are nearly identical. Third, both the G2(MP2) total energies and the relative energies (including heat of reaction and potential barrier) are nearly the same at three types of optimized geometries for all species. This result can be expected since both the geometrical parameters and the frequencies show little change.

In summary, the characteristic of potential energy surface for the $Cl + CH_2CO$ system is effectively independent of the basis sets used in the optimization. Moreover, Table 2 shows that a quite good agreement with the experimental heats of reaction is also found in the case of the MP2(full) calculations, with the exception of channel II (HCl + HCCO). These results support

that the UMP2(full)/6-31G(d,p) level of theory might be quantitatively adequate to characterize the potential energy surface of the Cl + CH_2CO reaction.

4. The Rate Constants for Key Product Channels. The UMP2(full)/6-31G(d,p) optimized geometries and vibrational frequencies and the G2(MP2) energies were employed to estimate the kinetics of the Cl + CH_2CO reaction.

A. Mechanism and Formula. We have calculated the rate constants for various product channels according to the following *simplified* mechanism which, however, has included all the most important channels:

$$\mathrm{Cl+CH_2CO} \underset{2}{\overset{1}{\rightleftharpoons}} (\mathrm{P}\pi\mathrm{C})^* \xrightarrow{w_1} \mathrm{P}\pi\mathrm{C}$$

$$\xrightarrow{3} \mathrm{HCl+HCCO}$$

$$\underset{5}{\overset{4}{\rightleftharpoons}} (\mathrm{CH_2ClCO})^* \xrightarrow{8} \mathrm{CO+CH_2Cl}$$

$$\xrightarrow{w_2} \mathrm{CH_2ClCO}$$

$$\underset{7}{\overset{6}{\rightleftharpoons}} (\mathrm{CH_2CClO})^* \xrightarrow{w_3} \mathrm{CH_2CClO}$$

where "*" represents the vibrational excitation of the PπC, CH_2ClCO, and CH_2CClO intermediates. Steady-state assumption for all excited intermediates leads to the following expressions for the second-order rate constants of various product channels:

$$k_{\mathrm{CO+CH_2Cl}} = \kappa\frac{\alpha_1}{h}\frac{Q_t^{\ddagger}Q_r^{\ddagger}}{Q_{\mathrm{Cl}}Q_{\mathrm{CH_2CO}}}e^{-E_1/KT}\int_0^{\infty}\frac{k_8(E)\,X_2(E)W_1(E^{\ddagger})}{Y(E)}e^{-E^{\ddagger}/KT}\,dE^{\ddagger} \quad (1)$$

$$k_{\mathrm{HCl+HCCO}} = \kappa\frac{\alpha_1}{h}\frac{Q_t^{\ddagger}Q_r^{\ddagger}}{Q_{\mathrm{Cl}}Q_{\mathrm{CH_2CO}}}e^{-E_1/KT}\int_0^{\infty}\frac{k_3(E)\,W_1(E^{\ddagger})}{Y(E)}e^{-E^{\ddagger}/KT}\,dE^{\ddagger} \quad (2)$$

$$k_{\mathrm{P}\pi\mathrm{C}} = \kappa\frac{\alpha_1}{h}\frac{Q_t^{\ddagger}Q_r^{\ddagger}}{Q_{\mathrm{Cl}}Q_{\mathrm{CH_2CO}}}e^{-E_1/KT}\int_0^{\infty}\frac{\omega_1 W_1(E^{\ddagger})}{Y(E)}e^{-E^{\ddagger}/KT}\,dE^{\ddagger} \quad (3)$$

$$k_{\mathrm{CH_2ClCO}} = \kappa\frac{\alpha_1}{h}\frac{Q_t^{\ddagger}Q_r^{\ddagger}}{Q_{\mathrm{Cl}}Q_{\mathrm{CH_2CO}}}e^{-E_1/KT}\int_0^{\infty}\frac{\omega_2 X_2(E)\,W_1(E^{\ddagger})}{Y(E)}e^{-E^{\ddagger}/KT}\,dE^{\ddagger} \quad (4)$$

$$k_{\mathrm{CH_2CClO}} = \kappa\frac{\alpha_1}{h}\frac{Q_t^{\ddagger}Q_r^{\ddagger}}{Q_{\mathrm{Cl}}Q_{\mathrm{CH_2CO}}}e^{-E_1/KT}\int_0^{\infty}\frac{\omega_3 X_3(E)\,W_1(E^{\ddagger})}{Y(E)}e^{-E^{\ddagger}/KT}\,dE^{\ddagger} \quad (5)$$

where

$$k_i(E) = \alpha_i C_i W_i(E_i^{\ddagger})/N_j(E_j) \quad (6)$$

$$Y(E) = X_1(E) - X_2(E)\,k_5(E) - X_3(E)\,k_7(E) \quad (7)$$

$$X_1(E) = k_2(E) + k_3(E) + k_4(E) + k_6(E) + w_1 \quad (8)$$

$$X_2(E) = k_4(E)/[k_5(E) + k_8(E) + w_2] \quad (9)$$

$$X_3(E) = k_6(E)/[k_7(E) + w_3] \quad (10)$$

and

$$w = \beta_c Z_{\mathrm{LJ}}[\mathrm{M}] \quad (11)$$

In the above equations, α_i is the statistical factor for the *i*th reaction path, and E_1 is the energy barrier for the formation of PπC via step 1. In our case, $E_1 = 0$. Q_{Cl} and $Q_{\mathrm{CH_2CO}}$ are the total partition functions of Cl and CH_2CO, respectively. It is noted that the electronic partition function of Cl(^{2}P) is $Q_e = 4 + 2\exp(-1268/T)$. $Q_t^{\ddagger}$ and $Q_r^{\ddagger}$ are the translational and rotational partition functions of "transition state" for the formation of PπC, respectively. $W_1(E^{\ddagger})$ is the sum of states of this "transition state" with excess energy $E^{\ddagger}$ above the association barrier. $k_i(E)$ is the energy-specific rate constant for the *i*th channel, and C_i is the ratio of the overall rotational partition function of the transition state for the *i*th channel (i = 2, 3, 4, 5, 6, 7, 8) and the *j*th intermediate (j = 1, 2, 3 for PπC, CH_2ClCO, CH_2CClO, respectively). w_j is the effective collision frequency for the *j*th intermediate. β_c is the collision efficiency which is calculated by Troe's weak-collision approximation.[31] Z_{LJ} is the Lennard-Jones collision frequency, and [M] is the concentration of the bath gas M.

B. Assumptions and Uncertainty. The following approximations have been taken into account in the present multichannel RRKM−TST calculations:

(i) The direct hydrogen abstraction channel, the formation of H + CHClCO and CHClCHO from CH_2ClCO, and the possible reaction channels involving the electronically excited species were omitted. As mentioned above, all these channels are energetically unfavorable. So long as the temperature is not extremely high, they cannot contribute significantly to the overall reaction since the rate constants were calculated only at temperatures between 300 and 1500 K.

(ii) The hydrogen-bonded complex HBC1 between HCl and HCCO has not been included in the *simplified* reaction mechanism. Because the decomposition of HBC1 into HCl and HCCO has no well-defined transition state, at present, our multichannel RRKM program is incapable of dealing with this kind of reaction path. Since the binding energy of HBC1 is relatively small, HBC1 cannot remain bound at higher temperatures. The neglect of this weakly bonded complex in the kinetic calculation should be acceptable.

(iii) There might exist a 1,2-C1 shift channel from CH_2ClCO(^{2}A′) to CH_2CClO(^{2}A″). Unfortunately, all our attempts to locate the corresponding transition state for this rearrangement pathway were shown to be futile. Various possible optimizations either do not converge or lead to the transition state TS2. We have to reserve this open question for future study. The existence of such a path would reduce the RRKM-predicted yield of CH_2CClO and perhaps increase the yield of HCl + HCCO.

(iv) The quantum tunneling correction was omitted. This simplification should not pose a problem, as there is no barrier to reaction, and all but one transition state (TS3) is below reagent energy. However, the HCl elimination from PπC may have significant tunneling as indicated by the large imaginary frequency of TS3. Fortunately, this channel is of no importance because it involves a high-energy barrier. Therefore, the rate constant for this channel may be still qualitatively reasonable even though it might be underestimated especially in lower temperatures.

(v) The formations of CH_2ClCO(^{2}A′) and CH_2CClO(^{2}A″) from PπC were considered to involve the "tight" transition states (i.e., TS1 and TS2), but the corresponding barrier heights were taken as equal to zero. This assumption is based on two facts: TS1 disappears at the higher level computation; the energy of TS2 is only 0.9 kcal/mol higher than that of PπC, and this value is even smaller than the average absolute deviation (±2 kcal/

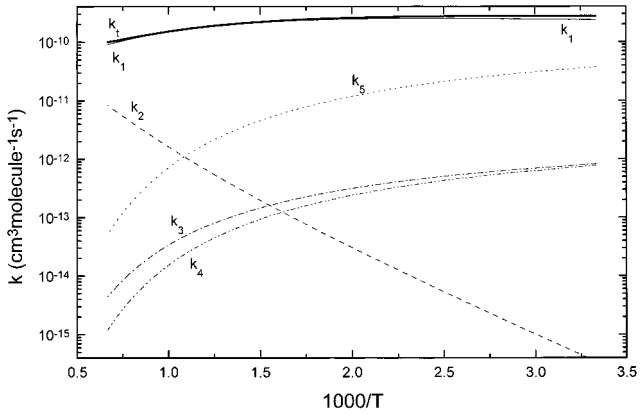

Figure 4. Arrhenius plot of the total rate constants (k_t) for the Cl + CH_2CO reaction and the individual rate constants for various product channels at 760 Torr pressure of N_2. k_1, k_2, k_3, k_4, and k_5 represent the rate constant for the formation of CO + CH_2Cl, HCl + HCCO, PπC, CH_2ClCO, and CH_2CClO, respectively.

mol) of the G2(MP2) energy. Certainly, this assumption can overestimate the yield of CH_2CClO.

(vi) As the Lennard-Jones parameters for the intermediates involved in all the reaction paths are not available in the literature, the estimated data, $\epsilon = 200$ K and $\sigma = 5.0$ Å, were used to calculate the collision frequency factor Z_{LJ}. Furthermore, we assumed that Z_{LJ} is the same for all the intermediates. This approximation could not cause the significant error for the temperature range of interest since the same simplification has been successfully applied in many multichannel RRKM calculations.[32,33]

(vii) The "transition state" for the process 1 or 2 cannot be determined readily by ab initio calculation because of the absence of a well-defined reaction barrier. In principle, the evaluation of the rate constant for process 1 or 2 can be carried out using the canonical variational transition state methods (CVT)[34−36] with the potential energy curve in Figure 3. However, the CVT method is too complex to be employed in our multichannel RRKM program, and most importantly, the UMP2 level (even higher levels of theory) cannot be quantitatively adequate to deal with the weak long-range interaction between Cl and CH_2CO. In addition, the essential molecular parameters such as vibrational frequencies and moment of inertia of the internal rotation cannot be determined readily. Therefore, we employed a simpler alternative method, namely "loose transition state" (LST) model, in the present multichannel rate calculation. The LST method has been widely used to model the kinetics for many barrierless reactions.[28,37] The "transition state" for the association of Cl with CH_2CO is assumed to have two free internal rotors and the same vibrational frequencies as the reactant CH_2CO. The average moment of inertia of the internal rotor was determined to be 7.3 amu by fitting the experimental rate constant at 295 K, $k_t = 2.7 \times 10^{-10}$ cm^3 molecule^{-1} s^{-1}.

In view of all these approximations, together with other possible systematic errors (e.g., the uncertainty of energies, the omission of vibrational anharmonicity, and angular momentum conservation) and the extent of error propagation or cancellation, the calculated rate constants easily have 50% or larger uncertainty.

C. Reliability of the RRKM Simulation. Despite the inevitable large uncertainty, the present RRKM calculation should be reliable because it can reproduce exactly the following experimental results: (i) At $T = 295$ K, the overall rate constants are pressure independent in the range 1−700 Torr of N_2.[10] For

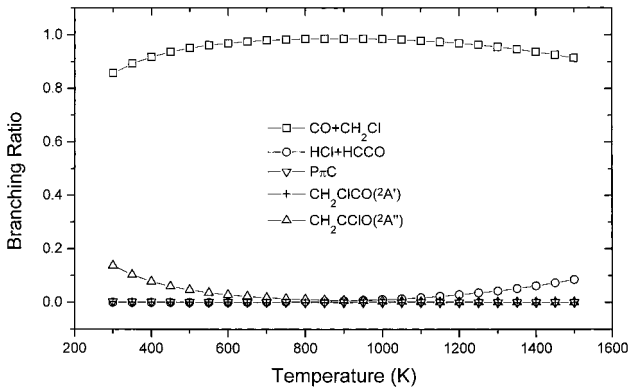

Figure 5. Temperature dependence of the branching ratios for various product channels. The branching ratios of PπC and $CH_2ClCO(^2A')$ are both effectively zero.

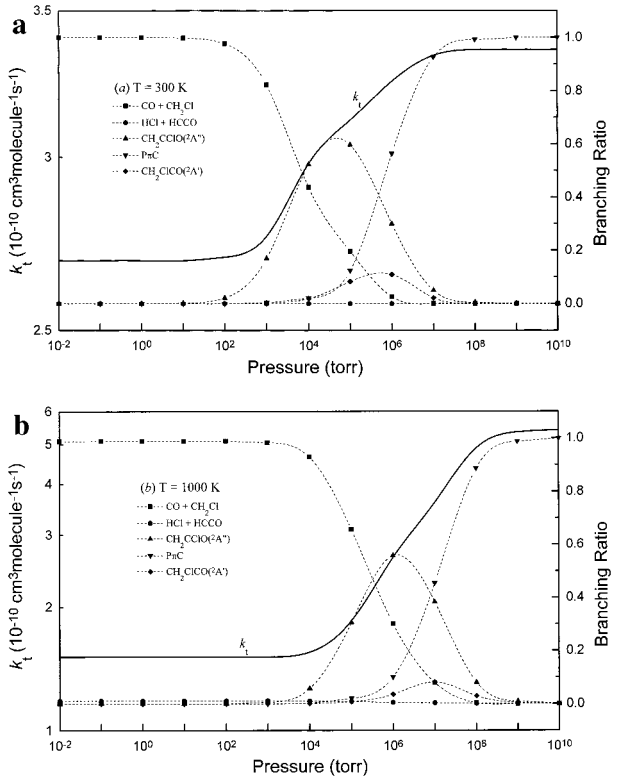

Figure 6. Pressure dependence of the total rate constants (solid lines) and branching ratios of various product channels (short dashed lines with various symbols) in the Cl + CH_2CO reaction at (a) 300 and (b) 1000 K, respectively.

example, at $P = 1$, 100, and 700 Torr, the calculated rate constants are all 2.7×10^{-10} cm^3 molecule^{-1} s^{-1}. (ii) From 235 to 353 K, the rate constants show little change.[11] (iii) At 1−2 mbar of He and $T = 300$ K, the major products are CO and CH_2Cl with a branching ratio of ∼1.0. The other products are negligible. (iv) The overall constants exhibit negative temperature dependence between 300 and 1500 K. Although there is no direct experimental evidence for this result, the negative temperature dependence of the total rate constants has been observed in several analogous reactions of CH_2CO with OH,[7] CN, and NCO.[14]

D. A Few Predictions. RRKM calculations have been performed for atmospheric pressure with N_2 as the bath gas over the temperature range of 300−1500 K. The total and individual rate constants and the branching ratios are shown in Figures 4 and 5, respectively. The pressure dependence of the overall rate

constants and branching ratios for various channels at two temperatures (300 and 1000 K) are depicted in Figure 6.

Figure 4 shows the negative temperature dependence of the overall rate constants. The individual rate constants k_1, k_3, k_4, and k_5 decrease monotonically whereas k_2 increases rapidly with the elevated temperatures. The total rate constants are fitted by least squares to the following three-parameter expression for 300−1500 K and 760 Torr of N_2:

$$k_t(\mathrm{cm^3\ molecule^{-1}\ s^{-1}}) = (1.0 \pm 0.2) \times 10^{-15} T^{-1.58\pm0.02} \exp(-565 \pm 2/T)$$

Figure 5 indicates that the major products are CO + CH_2Cl in the whole temperature range of interest. However, at lower temperatures CH_2CClO also has a certain branching ratio. At higher temperatures the minor products HCl and HCCO can be formed. The branching ratios of PπC and CH_2ClCO are both negligible.

Figure 6 exhibits the typical falloff behavior for the complex-forming reactions. At $T = 300$ K, the falloff region of the total rate constants ranges from 10^3 to 10^7 Torr. At $T = 1000$ K, the falloff region moves to higher pressures (10^4−10^8 Torr). Meanwhile, it can be seen from Figure 6 that the major products are CO and CH_2Cl at lower pressures. At the high-pressure limit, PπC becomes the major product; that is, the stabilization of the intermediate PπC dominates the reaction. It is interesting to note that CH_2CClO has a significant branching ratio at 10^5−10^6 Torr. The formation of CH_2ClCO is also possible at 10^6−10^7 Torr, but again there is a significant uncertainty in these results.

V. Concluding Remarks

In this paper we report the most important reaction pathways for the reaction of Cl(^{2}P) with CH_2CO (ketene) at both the UMP2(full)/6-31G(d,p) and G2(MP2) levels of theory. The interesting results in the study of reaction mechanism are the following: (i) The reaction is dominated by the addition−elimination mechanism. The hydrogen abstraction pathway is negligible. (ii) The addition reaction starts by the formation of a p−π complex (PπC). The binding energy of PπC is 10.1 kcal/mol. (iii) PπC can rearrange to CH_2ClCO or CH_2CClO without barrier, or decompose into HCl and HCCO via a high-energy barrier and a weakly hydrogen bonded complex (HBC1). (iv) The dominant reaction channel of CH_2ClCO is the CC bond scission, forming CO and CH_2Cl.

Using multichannel RRKM−TST procedure and ab initio data, we have calculated the rate constants and branching ratios at various temperatures and pressures. The "loose transition state" model was employed in the treatment of the barrierless reaction entrance. The good agreement of the theoretical values with the reported experimental results demonstrates that the calculated rate constants are reliable and thus the reaction mechanism is valid. The major findings in the kinetic calculations are (i) the total rate constants have negative temperature dependence and falloff behavior; and (ii) at lower pressures (P $< 10^3$ Torr), the major products are always CO and CH_2Cl over the whole temperature range of interest.

Acknowledgment. The authors thank two referees for their valuable comments and Mr. A. Vahid for his improvement of the English of the manuscript.

Supporting Information Available: Tables 1S lists the *Z*-matrixes for various intermediates and transition states involved in this work. Figures 1S and 2S show the potential surfaces for the CCl bond cleavage of $CH_2CClO(^2A'')$ and the hydrogen abstraction of CH_2CO by Cl, respectively. This information is available free of charge via the Internet at http://pubs.acs.org.

References and Notes

(1) Michael, J. V.; Nava, D. F.; Payne, W. A.; Stief, L. J. *J. Chem. Phys.* **1979**, *70*, 5222.
(2) Slemr, F.; Warneck, P. *Ber. Bunsen-Ges. Phys. Chem.* **1957**, *79*, 152.
(3) Umemoto, H.; Tsunashima, S.; Sato, S.; Washida, N.; Hatakeyama, S. *Bull. Chem. Soc. Jpn.* **1984**, *57*, 2578.
(4) Washida, N.; Hatakeyama, S.; Takagi, H.; Kyogoku, T.; Sato, S. *J. Chem. Phys.* **1983**, *78*, 4533.
(5) Gaffnay, J. S.; Atkinson, R.; Pitts, J. N., Jr. *J. Am. Chem. Soc.* **1975**, *97*, 5049.
(6) Oehlers, C.; Temps, F.; Wagner, H. Gg. Wolf, M. *Ber. Bunsen-Ges. Phys. Chem.* **1992**, *96*, 171.
(7) Brown, A. C.; Canosa-mas, C. E.; Parr, A. D.; Wayne, R. *Chem. Phys. Lett.* **1989**, *161*, 491.
(8) Hatakeyama, S.; Honda, S.; Washida, N.; Akimoto, H. *Bull. Chem. Soc. Jpn.* **1985**, *58*, 2157.
(9) Ebrecht, J.; Hack, W.; Wagner, H. Gg. *Ber. Bunsen-Ges. Phys. Chem.* **1990**, *94*, 587.
(10) Wallington, T. J.; Ball, J. C.; Straccia, A. M.; Hurley, M. D.; Kaiser, E. W.; Dill, M.; Schneider, W. F. *Int. J. Chem. Kinet.* **1996**, *28*, 627.
(11) Marico, M.; Ball, J. C.; Straccia, A. M.; Szente, J. J. *Int. J. Chem. Kinet.* **1997**, *29*, 421.
(12) Grussdorf, J.; Temps, N. F.; Wagner, H. Gg. *Ber. Bunsen-Ges. Phys. Chem.* **1994**, *98*, 546.
(13) Hudgens, J. W.; Dulcay, C. S.; Long, G. R.; Bogan, D. *J. Chem. Phys.* **1987**, *87*, 4546.
(14) Edwards, M. A.; Hershberger, J. F. *Chem. Phys.* **1998**, *234*, 231.
(15) Curtiss, L. A.; Raghavachari, K.; Redfern, P. C.; Pople, J. A. *J. Chem. Phys.* **1997**, *106*, 1063.
(16) DeMore, W. B.; Sander, S. P.; Golden, D. M.; Hampson, R. F.; Kurylo, M. J.; Howard, C. J.; Ravishankara, A. R.; Kolb, C. E.; Molina, M. J. *Chemical Kinetics and Photochemical Data for Use in Stratospheric Modeling*; JPL Publication 97-4; NASA: CA, 1997.
(17) Frisch, M. J.; Trucks, G. W.; Schlegel, H. B.; Gill, P. W. M.; Johnson, B. G.; Robb, M. A.; Cheeseman, J. R.; Keith, T. A.; Petersson, G. A.; Montgomery, J. A.; Raghavachari, K.; Allaham, M. A.; Zakrzewski, V. G.; Ortiz, J. V.; Foresman, J. B.; Cioslowski, J.; Stefanov, B. B.; Nanayakkara, A.; Challacombe, M.; Peng, C. Y.; Ayala, P. Y.; Chen, W.; Wong, M. W.; Andres, J. L.; Replogle, E. S.; Gomperts, R.; Martin, R. L.; Fox, D. J.; Binkley, J. S.; Defrees, D. J.; Baker, J.; Stewart, J. P.; Head-Gordon, M.; Gonzales, C.; Pople, J. A. *Gaussian 94*, Revision E.1; Gaussian Inc.: Pittsburgh, PA, 1995.
(18) Mϕller, C.; Plesset, M. S. *Phys. Rev.* **1934**, *46*, 618.
(19) Kwiatkowski, J. S.; Leszczynski, J. *J. Mol. Struct. (THEOCHEM)* **1995**, *342*, 43.
(20) Hehre, W.; Radom, L.; Schleyer, R. v. R.; Pople, J. A. *Ab Initio Molecular Orbital Theory*; Wiley: New York, 1986.
(21) Gonzalez, C.; Schlegel, H. B. *J. Chem. Phys.* **1989**, *90*, 2154.
(22) Gonzalez, C.; Schlegel, H. B. *J. Phys. Chem.* **1990**, *94*, 5523.
(23) Ignatyev, I. S.; Xie, Y.; Allen, W. D.; Schaefer, H. F. *J. Chem. Phys.* **1997**, *107*, 141.
(24) Schlegel, H. B.; Sosa, C. *Chem. Phys. Lett.* **1988**, *145*, 329.
(25) Farnell, L.; Pople, J. A. Radom, L. *J. Phys. Chem.* **1983**, *87*, 79.
(26) McDouall, J. J. W.; Schlegel, H. B. *J. Chem. Phys.* **1989**, *90*, 2363.
(27) Curtiss, L. A.; Raghavachari, K.; Pople, J. A. *J. Chem. Phys.* **1993**, *98*, 1293.
(28) Berman, M. R.; Lin, M. C. *J. Phys. Chem.* **1983**, *87*, 3933.
(29) Robinson, P. J.; Holbrook, K. A. *Unimolecular Reaction*; Wiley: New York, 1972.
(30) Jorgenson, W. L.; Salem, L. *The Organic Chemists Book of Orbitals*; Academic Press: New York, 1973; p 124.
(31) Troe, J. *J. Phys. Chem.* **1979**, *83*, 114.
(32) Marchand, N.; Rayez, J. C.; Smith, S. C. *J. Phys. Chem. A* **1998**, *102*, 3358.
(33) Wang, B.; Hou, H.; Gu, Y. *J. Phys. Chem. A* **1999**, *103*, 8021.
(34) Garret, B. C.; Truhlar, D. G. *J. Chem. Phys.* **1979**, *70*, 1593.
(35) Isaacson, A. D.; Truhlar, D. G. *J. Chem. Phys.* **1982**, *76*, 1380.
(36) Mebel, A. M.; Diau, E. W. G.; Lin, M. C. Morokuma, K. *J. Am. Chem. Soc.* **1996**, *118*, 9759.
(37) Lin, M. C.; He, Y.; Melius, C. F. *J. Phys. Chem.* **1993**, *97*, 9124.